Eur. Phys. J. D **45**, 491–499 (2007)
DOI: 10.1140/epjd/e2007-00248-8

THE EUROPEAN PHYSICAL JOURNAL D

Mapping the femtosecond dynamics of supported clusters with nanometer resolution

M. Rohmer[1,a], F. Ghaleb[2], M. Aeschlimann[1], M. Bauer[3], and H. Hövel[2]

[1] Department of Physics, TU Kaiserslautern, 67663 Kaiserslautern, Germany
[2] Experimentelle Physik I, Universität Dortmund, 44221 Dortmund, Germany
[3] Institut für Experimentelle und Angewandte Physik, Universität Kiel, 24118 Kiel, Germany

Received 7 February 2007 / Received in final form 20 June 2007
Published online 1st August 2007 –

Abstract. In this paper we present a combined STM, SEM and time-resolved PEEM study of silver clusters on a nano-patterned HOPG-substrate, exhibiting areas of different defect type and defect densities. The areas show small but distinct differences in the femtosecond dynamics associated with electronic excitations in the clusters. We assign these differences to variations in the cluster size distribution and variations in the cluster-substrate interaction as governed by the bonding to the different defect types.

PACS. 73.22.Lp Collective excitations – 79.60.Jv Interfaces; heterostructures; nanostructures – 61.46.+w Nanoscale materials: clusters, nanoparticles, nanotubes, and nanocrystals

1 Introduction

The ultrafast dynamics associated with the excitation of the electronic degrees of freedom in supported nanoparticles and clusters has been the focus of several studies in the past [1–6]. Frequency domain as well as time-domain measurements have been used to address the decay and dephasing of single electron excitations and collective (plasmon) excitations in these systems [7]. Of specific interest in some of these works has been the role of the support with respect to potential decay channels for these electronic excitations. A striking example is silver clusters on and embedded in SiO_2 where the cluster substrate interaction leads to a drastic change in the line width of the plasmon resonance [8]. Corresponding studies regarding the population decay of single electron excitations have been performed, for example, for silver clusters on nanostructured HOPG [4,9]. For a detailed understanding of the relevant mechanism in the cluster-substrate interaction, a controlled variation of the relevant substrate parameters is desirable. This involves, for instance, the preparation of defined defects as bonding sites for the clusters and their manipulation in terms of type, dimensionality or size. An experimental access to probe the differences in the ultrafast dynamics as governed by these modifications is difficult within a conventional (lateral integrating) spectroscopic scheme. Frequency domain measurements tend to be blurred by inhomogeneous broadening effects, whereas for time-domain measurements the typical lifetimes of electronic excitations of a few femtoseconds are very close to the temporal resolution that can be achieved with these techniques. The identification of any differences in the decay dynamics due to the substrate modifications is therefore a challenging task. One of the main sources limiting the sensitivity and the resolution of a technique are systematic errors in the measurements arising from undesired temporal drifts of the experimental parameters. Application of an experimental scheme that is capable of addressing the controlled substrate variations in a parallel fashion (at the same time) will enable the suppression of the influence of such systematic errors and will give rise to a significant improvement of the achievable resolution. Such an approach may involve a nano-structuring technique for a defined and highly local variation of relevant substrate parameters and a high resolution microscopy technique to achieve the required parallel data acquisition [10,11].

In this paper we present a combined scanning tunneling microscopy (STM), scanning electron microscopy (SEM), and time-resolved photoemission electron microscopy (TR-PEEM) study of silver clusters deposited on a HOPG (highly oriented pyrolytic graphite) substrate which has been locally manipulated by means of focused ion beam etching. We are able to show that the parallel acquisition mode of the PEEM enables us to resolve variations in the ultrafast cluster dynamics with a very high accuracy at a lateral resolution in the nanometer regime. Yet, the time-domain analysis of the data is performed in a qualitative manner by mapping the FWHM of the local two-photon photoemission autocorrelation trace. The method enables us to resolve changes in the FWHM of 1 fs and below. The interpretation of the mapped inhomogeneities in the local electron dynamics is possible because of the additional information obtained from the complementary SEM and STM measurements.

[a] e-mail: rohmer@physik.uni-kl.de

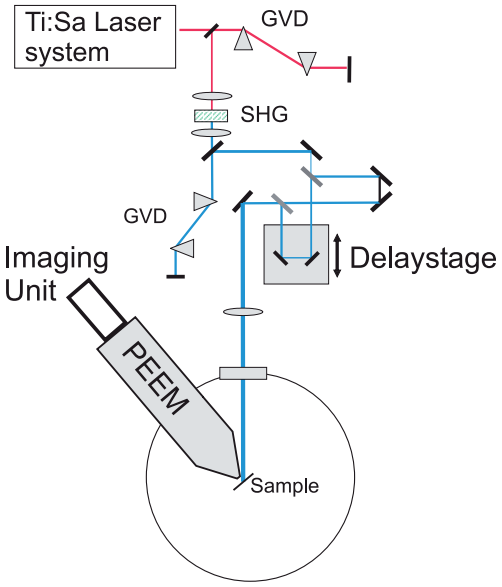

Fig. 1. Schematic view of the experimental set-up used for the time-resolved PEEM experiment.

2 Experimental set-up

A schematic view of the PEEM set-up used for the femtosecond studies at high lateral resolution is shown in Figure 1. The commercial PEEM instrument used for our experiments (Focus IS-PEEM) is described in detail in references [12,13]. The microscope is mounted in a μ-metal chamber to shield external stray magnetic fields that would affect the imaging quality of the system with respect to the lateral resolution. The optimum resolution that can be achieved with the microscope has been specified to <40 nm. The femtosecond dynamics associated with the electron excitations in the clusters can be addressed in the PEEM experiment using the time-resolved two-photon photoemission technique (TR-2PPE) [11]. A two-step excitation process involving intermediate excited electron states (single electron excitations and/or collective (plasmonic) excitations [6,14]) enables the access to the ultrafast dynamics associated with the dephasing and population decay of these kinds of excitations.

For the 2PPE we use a commercial pulsed femtosecond laser system (Spectra-Physics, Tsunami) that delivers 30 fs light pulses (FWHM) at 800 nm with a repetition rate of 80 MHz. These pulses are frequency doubled in a 0.2 mm thick BBO crystal to photon energy of 3.1 eV. To compensate for material induced group velocity dispersion (BBO crystal, air, focusing lenses and entrance viewport to the UHV chamber) and to achieve a minimum pulse length (30 fs corresponding to 45 fs FWHM of the measured autocorrelation trace) at the surface of the sample a pulse compressor consisting of a fused silica prism pair is used [15].

For the time-resolved measurements the 400 nm light pulses are split to equal intensity into pump and probe pulses. The probe pulse is temporally delayed with respect to the pump pulse by an optical delay stage. This computer controlled stage can be positioned with an accuracy of 100 nm corresponding to a temporal delay of 0.3 fs. After collinear combination of both beams by a second beam-splitter the light is finally focused onto the sample surface. The lateral resolution as offered by the PEEM enables one to adjust the spatial overlap of both beams at the sample surface with an accuracy of better than 5 μm at a spot diameter of about 150 μm.

The laterally resolved lifetime results obtained within a time-resolved PEEM experiment are visualized in so-called lifetime maps which are created as follows: For each pump-probe delay addressed within a time-resolved 2PPE scan, a corresponding Two-Photon-PEEM (2P-PEEM) image is recorded so that a time-series of PEEM images is produced (Fig. 2a). This time-series defines for each pixel a characteristic 2PPE-autocorrelation trace which contains the relevant information about the local electron dynamics (see Fig. 2b). A detailed, quantitative analysis of these traces requires a complex deconvolution procedure of the laser-autocorrelation. A qualitative picture of the involved femtosecond dynamics, which is particularly useful in comparing studies, can already be achieved from the full width at half maximum (FWHM) of the autocorrelation traces.

As a rule of thumb one finds that the FWHM of a trace increases as the excited state lifetime increases, where the broadening is typically of the order of the increase in the lifetime. Due to the large number of pixels per image and, hence, for autocorrelation traces to be analyzed per time-series, we restricted our data analysis to the latter approach which can be performed with a standard PC within a reasonable time-interval. A pixel-by-pixel plot of the FWHM of the autocorrelation trace enables us to produce a lifetime map of the sample as shown in Figure 2c for the case of a homogeneous 200 nm thick silver film. The measured FWHM of about 54 fs corresponds to an energy integrated excited state lifetime of about 10 fs. As evident from this lifetime map we observe a gradient in the local autocorrelation FWHM from the top right to the bottom left of the image. This gradient is observed for each time-series independent of sample material or sample structure and is therefore assigned to a characteristic feature of the laser pulses rather than to a characteristic of the sample. The gradient highlights a small spatial chirp of the incident laser beam (the dependence of the laser pulse width within the beam profile) most likely induced by inhomogeneities of the used UHV entrance window. It is of the order of only 3 fs over the entire beam diameter. All other lifetime maps which have been recorded under identical laser conditions have been corrected for this distortion. With this method we are able to resolve differences in the FWHM of the autocorrelation trace within a single map with an accuracy of better than 1 fs.

For characterization of the surface and the nanometer sized pits we used a low temperature Scanning Tunneling Microscope [16]. For stable imaging it was used at liquid nitrogen temperature. The silver evaporation was accomplished with a Knudsen cell-type evaporation source and a quartz thickness monitor. After

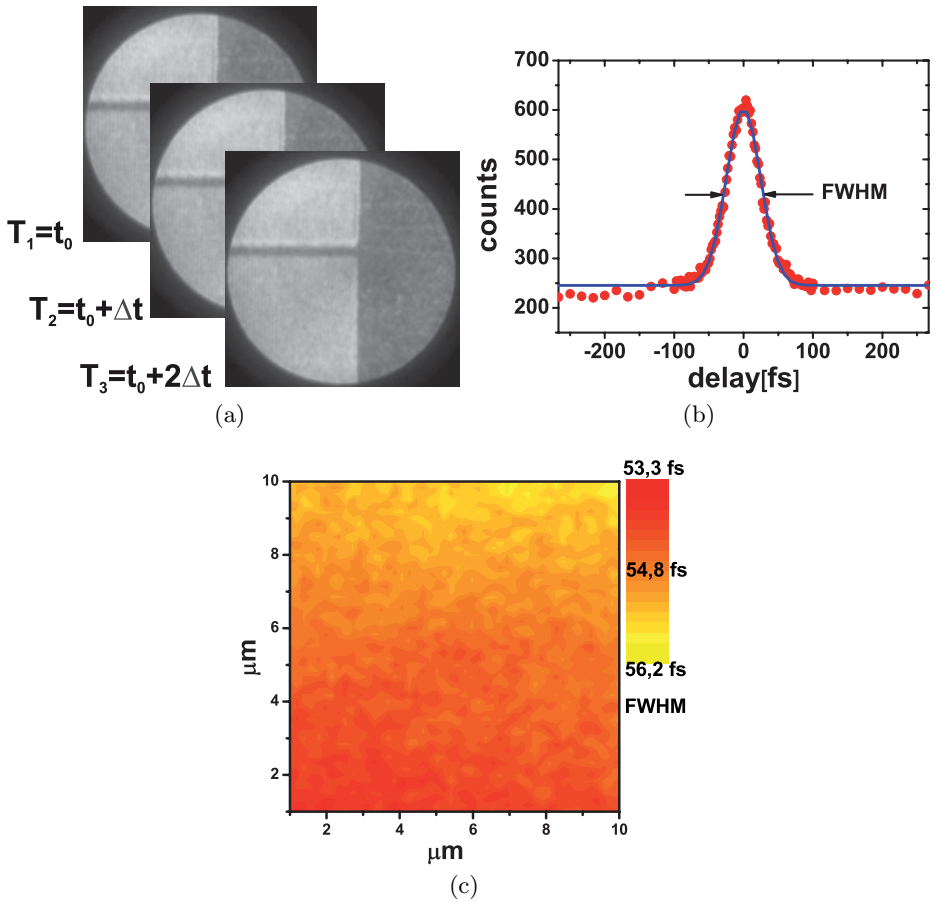

Fig. 2. Principle scheme of the time-resolved PEEM experiment (a) PEEM images are recorded at different temporal delays between the femtosecond pump and probe laser pulse. From this image series pump-probe autocorrelation traces for each pixel can be extracted. (b) The FWHM of these trace is taken as a qualitative measure for the probed ultrafast electron dynamics. (c) The color coded plot of these FWHM values at the corresponding pixel position maps the local variation of the femtosecond dynamics of the imaged surface within a laterally resolved life-time map (homogeneous silver film).

the TR-PEEM experiment, high resolution Scanning-Electron-Microscopy images were recorded with a commercial SEM system (Raith e-LiNE, 1540 Gemini Column, with 5 kV).

3 Sample preparation

The HOPG substrate used for our investigations exhibits several micrometer sized areas, each covered with nano-pits of characteristic size and density. These areas are interrupted by regions of native HOPG. With this sample it is possible to address cluster properties in interaction with varying substrate conditions in a parallel experimental approach (as offered by the PEEM technique). The main steps for the nano-pit production consist of a production of a defined density of atomic defects in the graphite surface with the focused ion beam technique (FIB) and a subsequent oxidation procedure following reference [17]. The ions in the FIB instrument (Raith ionLiNE) are produced with a Liquid-Metal Ion Source (LMIS) using gallium [18,19]. The ion beam is focused on the substrate and is then deflected laterally to perform the pre-programmed nano-patterning on the sample. The FIB-column is capable of a resolution below 10 nm. Following the FIB treatment the HOPG samples are oxidized in an oven (which has been cleaned in nitrogen atmosphere at 1000 °C before inserting the sample). The oxidation procedure is performed for 200 min at a well defined temperature of 540 °C in an Ar/O_2 mixture (2% oxygen). By maintaining a constant gas flow rate across the oven the oxygen density is kept constant and leads to a controlled growth of the nano-pits up to a diameter of a few nanometers. The pits for the samples used here have a statistical variation in their depth between 1 to 3 ML. More details about the FIB technique and the oxidation procedure can be found in references [20–22]. Two different nano-structured areas have been investigated in this study (sample 1, see Fig. 3a and sample 2, see Fig. 3b). Sample 1 (sample 2) has been written in a point pattern structure at a dose of 120 ions (480 ions) per point with 150 nm (300 nm) periodicity. After oxidation, the topography of the resulting nano-structured HOPG surfaces is examined with scanning tunneling microscopy (STM). Figure 3a shows a STM image of sample 1. Two distinct pit size regimes can be distinguished: pits of a diameter between 5–20 nm which appear with a density of $100/\mu m^2$ and pits in the size regime below 5 nm diameter with a density of $900/\mu m^2$. Figure 3b is a STM image of sample 2 (after oxidation). For this area a clear periodic structure is visible, which is caused by the line by line scan of the ion beam at a periodicity of 300 nm during the writing process. Within a written line, which is 150 nm wide, the 5–20 nm diameter pits appear with a density of $400/\mu m^2$, the 5 nm diameter

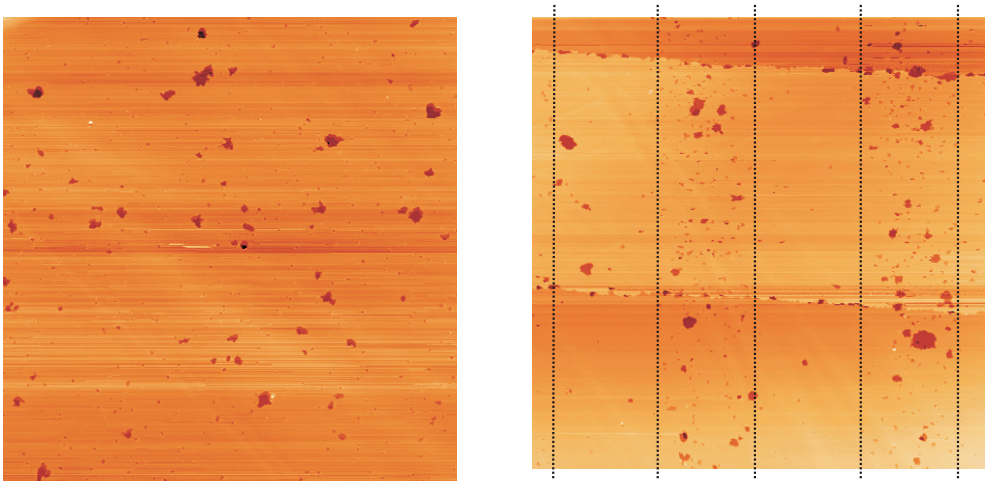

(a) (b)

Fig. 3. (a) 700×700 nm^2 STM image within sample 1 of the nano-patterned sample exhibiting two characteristic pit sizes. Pits in the size regime between 5 nm and 20 nm diameter appear at a density of 100/μm^2, pits with a diameter below 5 nm appear at a density of 900/μm^2. (b) A 700 × 700 nm^2 STM image within sample 2. The lines that have been written with a periodicity of 300 nm in the initial FIB process are clearly visible as areas of increased pit density. These lines have a width of about 150 nm and exhibit two characteristic pit sizes similar to sample 1. The large pits are found at a density of 400/μm^2, the small pits are found at a density of 1500/μm^2. The depth of the pits varies between 1–3 ML.

pits appear with a density of 1500/μm^2. 2P-PEEM of the surface prior to the deposition of the silver clusters shows a slightly increased (however, overall very small) photoemissivity from the nanostructured areas in comparison to the native HOPG.

Evaporation of 4 monolayers (ML) of silver at room temperature results in the condensation of silver clusters in the native and the artificially created defects in the HOPG surface.

For high resolution imaging of the clusters we used SEM instead of STM. For silver evaporated at room temperature at native HOPG surfaces it is well known that a stable STM imaging of the surface is not possible due to the small binding energy and the corresponding high mobility of the silver clusters [23,24]. Figure 5a shows an SEM image of the cluster decorated HOPG surface at the border of sample 1 in comparison to a corresponding 2P-PEEM image (Fig. 5b). To the left of both images, the nanostructured areas are clearly visible where the pattern periodicity of 150 nm, due to the writing process, is well resolved in the SEM image. The region to the right as well as an interstitial area interrupting the nanostructured region correspond to the cluster decorated *native* HOPG. High Resolution SEM allows quantifying cluster size, cluster size distribution (see Figs. 4a, 4b, 4c and 4d) and cluster density. For cluster decoration of the nanostructured areas (native HOPG areas) we find a density of 800/μm^2 dominated by cluster diameters between 12 and 7 nm (200/μm^2, from 20 nm diameter to sizes below the resolution limit of the SEM). The nonlinear photoemissivity from both areas (nanostructured as well as native) after silver evaporation has increased by orders of magnitude in comparison to the undecorated surface. We therefore conclude that the photoemission signal as mapped within the 2P-PEEM experiment (e.g., Fig. 5b) originates dominantly from the silver clusters and not from the HOPG substrate. For sample 1 we are not able to resolve the 150 nm periodicity in the PEEM experiments. The limitation in the PEEM resolution arises from the reduced extractor voltage that could be applied between the sample and the entrance lens of the PEEM in the present experiment (max 5 kV as opposed to 15 kV in the optimum case). For voltages >5 kV, leakage currents due to field emission from macroscopic defects in other areas of the HOPG prevented the imaging of the sample. Clearly resolved, however, are steps of the HOPG in the native areas, which are decorated by silver clusters.

Figures 6a and 6b show corresponding SEM and 2P-PEEM images of the border region of sample 2, this time for identical regions of the sample. The 300 nm periodicity of the patterning is also resolved in the 2P-PEEM image. Furthermore, steps of the HOPG substrate decorated with Ag clusters (see lines labelled A, B and C) are clearly visible in the SEM image. Analysis of high resolution SEM images show that in this region the nanostructured areas (native HOPG areas) exhibit a cluster size distribution between 10 and 8 nm at a density of 1300/μm^2 (from 20 nm to below the resolution limit at a density of 200/μm^2).

4 TR-PEEM results and discussion

Figure 7a shows a lifetime map of the area marked in the 2P-PEEM image in Figure 5b. It is important to keep in mind that the lifetime map is a priori not related to the local photoemission yield distribution (2P-PEEM map). It is a measure for the local variations in the ultrafast dynamical response associated with the electronic excitations in the cluster as probed by the 2PPE autocorrelation

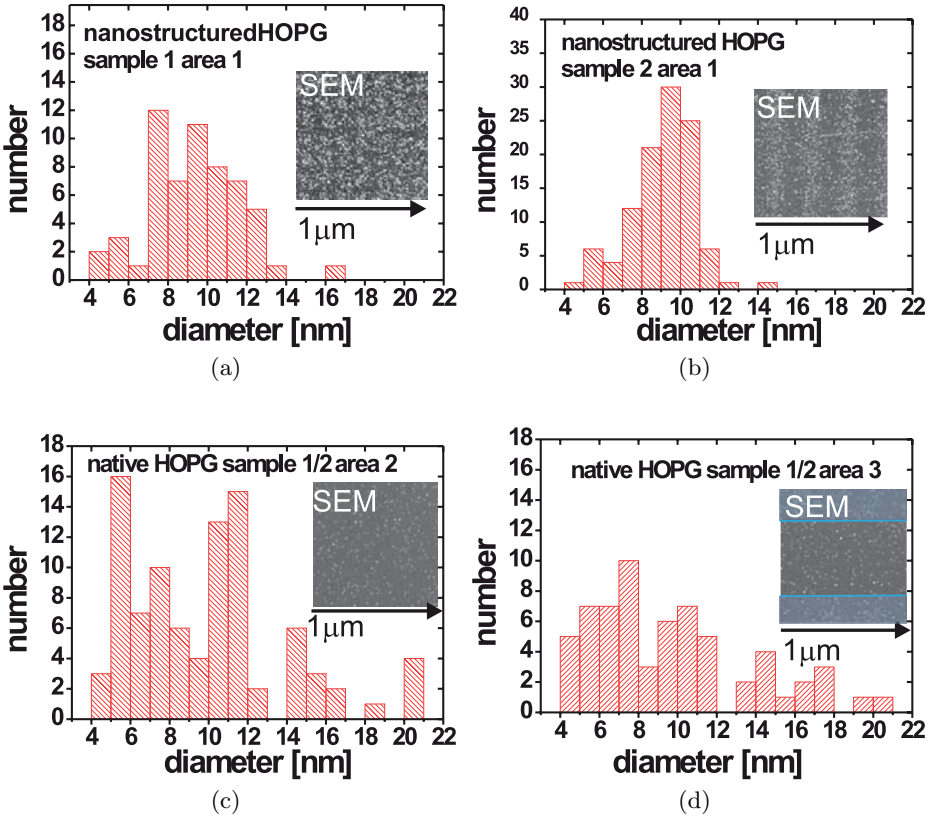

Fig. 4. Abundance spectra of the clusters at (a) nano-patterned sample 1 area 1, (b) nano-patterned sample 2 area 1, (c) native HOPG substrate area 2 (for both samples nearly identical) and (d) interstitial area 3 (for both samples nearly identical, the blue lines mark the boarder to the nano-patterned area; for the definition of areas 1, 2 and 3 see Fig. 7).

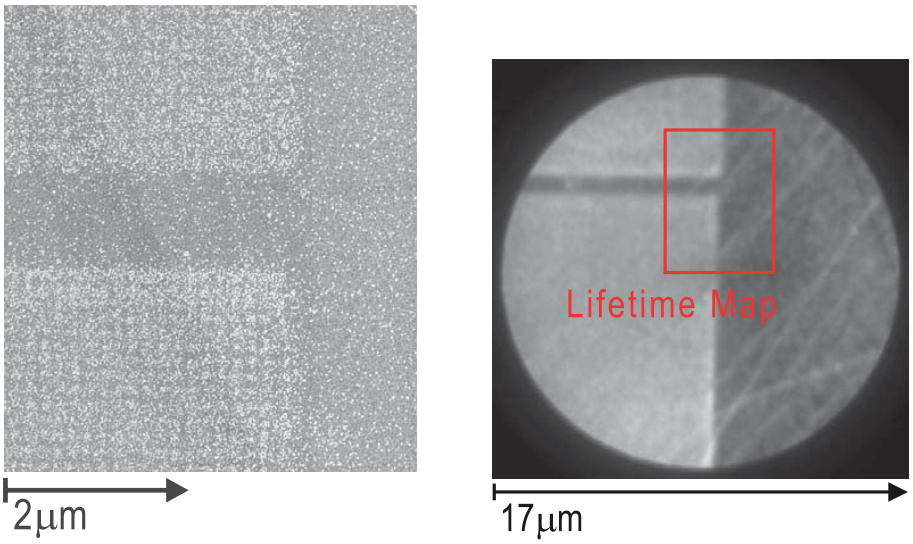

Fig. 5. (a) SEM image of the border region of sample 1 after cluster condensation. The nano-patterned area 1 corresponds to the two fields at the top left and bottom left of the image. (b) 2P-PEEM image of (another) border region of sample 1, the red rectangle marks the clipping displayed as lifetime-map in 7a).

trace. Even though this lifetime contrast is weak, the patterning of the structure as displayed in the SEM and the 2P-PEEM image is clearly reproduced. It is a direct proof that the interaction of the clusters with the different substrate properties offered by the nano-patterned HOPG affects the detailed electron dynamics of the silver clusters.

We are able to discriminate three different regions in the lifetime map: area 1 corresponding to the nano-structured area, area 2 corresponding to native areas at adequate distances from the nano-structured area, and area 3 corresponding to native HOPG areas in the close vicinity of the nano-structured areas.

The actual contrast mechanism responsible for the appearance of these regions in the lifetime map becomes more evident from a statistical analysis of the three regions as shown in Figure 7b. The three graphs display the distribution (histograms) of the FWHM pixel counts of the local autocorrelation traces for the respective regions.

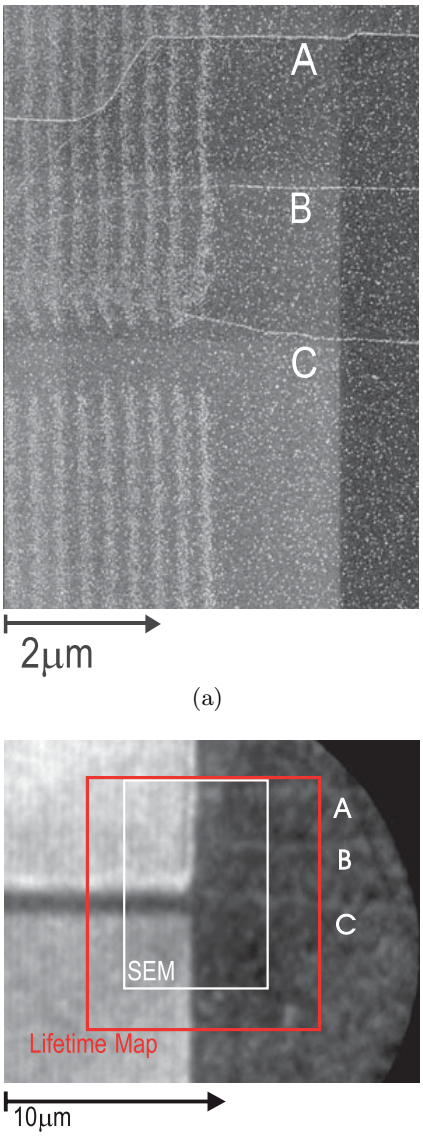

Fig. 6. (a) SEM image of the border region of sample 2 after cluster condensation. Clearly visible are the lines written in the FIB process with a periodicity of 300 nm. A, B, and C label steps in the HOPG substrate decorated with silver clusters at a high density. (b) 2P-PEEM image of the identical border region of sample 2 including the SEM imaged area (white rectangle in (b). The cluster decorated steps A, B, and C as well as the periodicity of the nano-structured region are well resolved. The red rectangle marks the clipping displayed as lifetime-map in 8a).

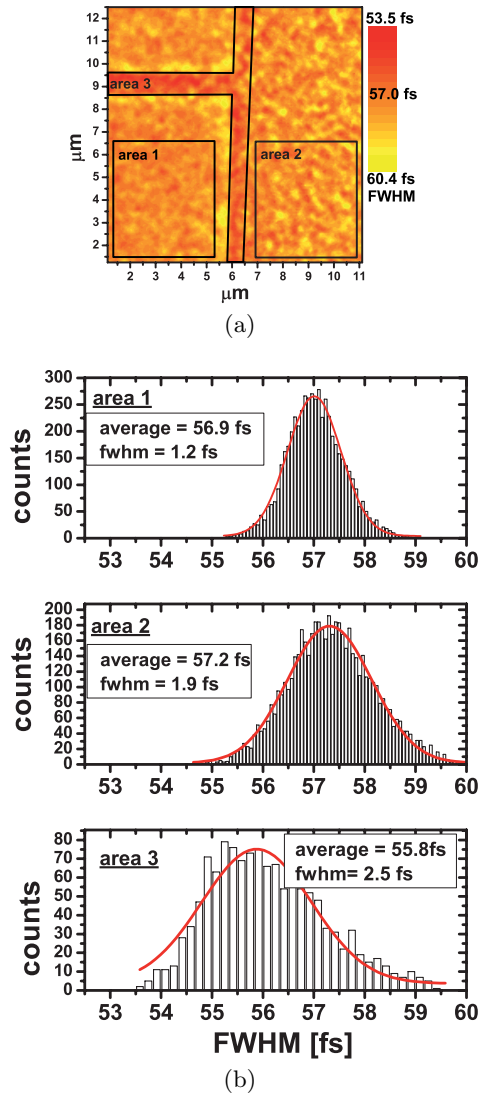

Fig. 7. (a) Lifetime map of the PEEM image clipping in Figure 5b (sample 1). The measured FWHM of the autocorrelation traces for every pixel vary among 53.5 fs and 60.4 fs. The three graphs in (b) show histograms of area 1, 2 and 3 marked in the lifetime map (fwhm = Histogram FWHM).

It enables us to discriminate two separate contrast mechanisms between different areas: The differences in the peak position of the FWHM distribution (corresponding to average lifetime) and the difference in the width of this distribution (variation of lifetime, fwhm = Histogram FWHM). A comparison between area 1 and area 2 shows, for instance, that the visible contrast arises rather from the distribution width (fwhm) than from the mean FWHM value of the autocorrelation trace. Area 3, in contrast, also shows a significant shift in the mean FWHM in comparison to area 2 and area 3. Note that the very small differences in the mean value and the width of the distribution of about 1 fs and even less can only be resolved due to the parallel data acquisition mode as offered by the PEEM technique. Only this approach guarantees that systematic errors within the measurements, for instance, due to drifts in the laser characteristics (pulse-width or spectrum) are completely cancelled out when comparing different areas. Similar lifetime contrast patterns as recorded for sample 1 are also observed in the sample 2 lifetime map as shown in Figure 8a. Again, a comparison between the structured (area 1) and unstructured (area 2) HOPG shows that the lifetimes contrast is dominated by the spread in the FWHM distribution

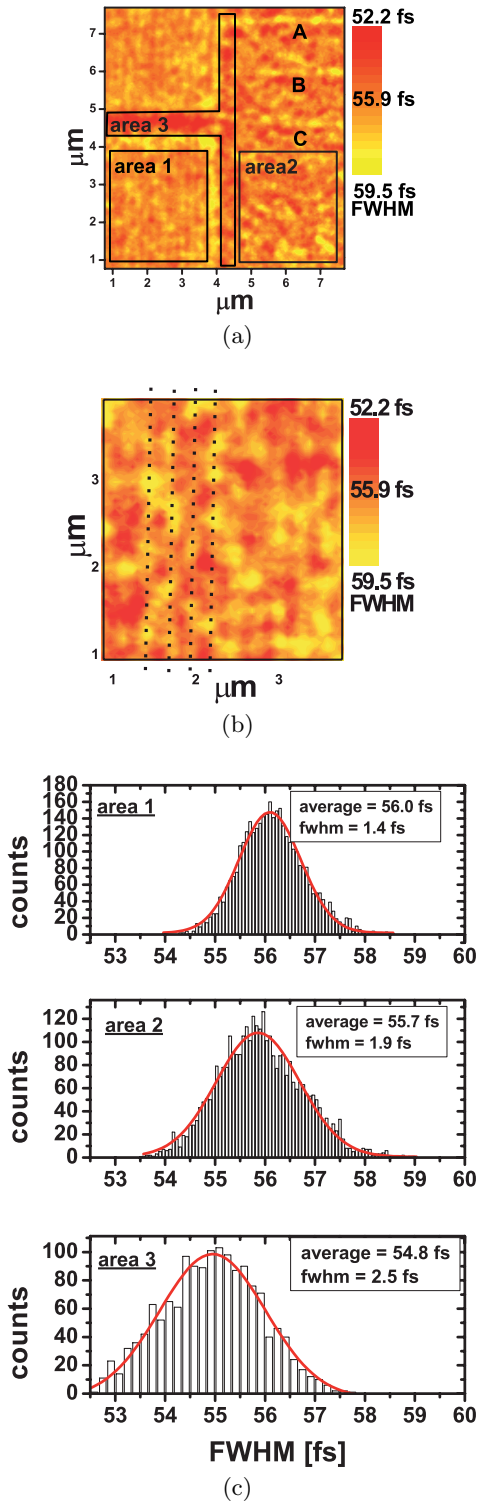

Fig. 8. (a) Lifetime map of the PEEM image clipping in Figure 6b. The measured FWHM of the autocorrelation traces for every pixel vary among 53.5 fs and 60.4 fs. The cluster decorated steps A, B, and C as well as the periodicity of the nano-structured region is visible as lifetime contrast. (b) Clipping of (a) showing area 1 with the 300 nm periodicity in the lifetime map. Dotted lines are added to guide the eye. The three graphs in (c) show histograms of area 1, 2 and 3 marked in the lifetime map (fwhm = Histogram FWHM).

(fwhm) rather than by the mean value (average of the histograms) of the FWHM. We also reproduce the shift of the mean value in area 3 to smaller FWHM values in comparison to area 1 and area 2. Two further points are noticeable in Figures 8a and 8b. Firstly, the periodicity of the structure pattern of 300 nm is resolved in the lifetime map, indicating different electron dynamics in the high density regions of the pattern structure in comparison to the low density regions. Furthermore, the step decorated areas labelled with A, B, and C in the SEM and the 2P-PEEM image give rise to a clear lifetime contrast. From the lifetime maps of the nano-patterned HOPG samples it is evident that the detailed electron dynamics of the silver clusters is governed by the properties of the underlying substrate. To gain insight into the relevant mechanism for these differences it is helpful to briefly review the kind of electron dynamics that is probed in a time-resolved 2PPE experiment. Conventionally, this technique is used to address the electron dynamics at a single crystalline surface. For these systems the 2PPE technique probes the dephasing and relaxation dynamics of single electron excitations such as bulk electron excitations [25], image states [26] or adsorbate excitations [27]. In the case of nanoscale metallic structures such as the silver clusters probed in this study, collective electronic excitations, so-called localized surface plasmons (LSP) also have to be considered for a complete description of the time-resolved 2PPE process. As shown by Pfeiffer and coworkers [5] the plasmon excitation governs the amplitude, the phase and the temporal width of the particle internal field induced by the incident laser pulse. It is this plasmon induced internal field which is responsible for the single electron excitation finally giving rise to the measured 2PPE yield. Consequently, the shape and width of the 2PPE autocorrelation from a silver cluster is determined by both the dynamics of the plasmon excitation as well as the dynamics of the single electron excitations. This involvement of different excitation scenarios makes a closed interpretation of the data at this point rather challenging. Still, particularly the comparison of the lifetime data with the SEM images allows for some first qualitative statements about the microscopic origin of the detected local lifetime variations.

The increased spread in the FWHM distribution for clusters supported by the native HOPG surface (see Figs. 7b, 8c area 2) in comparison to the nanostructured HOPG results (see Figs. 7b, 8c area 1) is clearly correlated with an increased spread in the cluster size distribution (histograms Figs. 4a, 4b, 4c, 4d). The decay dynamics of single electron excitations in clusters is governed by the detailed electronic structure of the cluster. However, for the investigated size regime the electronic structure can be considered to be bulk like and size independent so that it cannot account for any size (distribution) dependence in the probed femtosecond dynamics. The same argumentation is true for the Landau damping of the LSP mode, which accounts for the decay of a plasmon due to an electron-hole pair excitation in the cluster. An alternative decay channel for the LSP excitation is radiation damping, which corresponds to the loss of excitation energy by

the emission of coherent light induced by the collective (dipolar) oscillation of the electron cloud in the cluster. Radiation damping exhibits clear size dependence, scaling linearly with the volume of the cluster [3,28]. Even though radiation damping is not the dominant decay channel in the investigated cluster size regime it still may be sufficiently strong to account for the observed small difference between area 1 and area 2.

Of further interest is the periodic contrast modulation visible in the sample 2 at a periodicity of 300 nm reflecting the nano-pattering induced by the FIB treatment. Again it is possible to relate these lifetime variations to differences in the cluster size distribution. The average cluster size in a region is determined by the competition between evaporated material and the number of pits available for the condensation of a cluster. Therefore, for the same (nominal) silver coverage the low density pit areas of the grating should exhibit a larger mean cluster diameter than the areas of high pit density. A detailed inspection of high-resolution SEM images confirms this view. Following the discussion of the lifetime contrast between native and nano-structured HOPG areas, we therefore assign the grating modulation to the increased radiation damping of the large clusters in the low density areas. Note that such an interpretation agrees well with the dark appearance of these areas in the lifetime map corresponding to local autocorrelation traces with a small FWHM, indicative of slightly shorter lifetimes. In a similar manner we can also understand the bright appearance of the cluster decorated HOPG steps A, B, and C (see labelling in Figs. 5a and 5b) in the lifetime map. The SEM images give evidence for a high density condensation of clusters at these steps and consequently small cluster radii, which intrinsically exhibit a reduced coupling efficiency to the radiation damping channel.

Finally, we also would like to consider area 3 (in both lifetime maps) which gives rise to the most pronounced lifetime contrast in the lifetime map with respect to the FWHM mean value. Even though the analysis of the SEM images from this region indicates identical properties with respect to cluster size distribution and cluster density in comparison to the native HOPG area 2, a significant shift of the mean FWHM of the autocorrelation traces to smaller values is observed. Note also that in contrast to the lifetime maps the 2P-PEEM and SEM images do not show any specific contrast of this region with respect to the rest of the native HOPG. We conclude that the individual cluster properties cannot account for the observed contrast. It is therefore tempting to assign these modifications to the interaction of the cluster with the surrounding substrate. For plasmonic excitations of clusters it has been shown in the past that an efficient coupling to the substrate can significantly affect the lifetime [8]. Yet, this does not explain the contrast between area 2 and area 3 which are both supposed to be regions of native HOPG. However, it is likely that areas in the vicinity of the nano-pattered region become structurally and/or chemically modified by the FIB treatment of the sample. Such modifications may offer additional decay channels to the cluster excitations which then give rise to the observed lifetime quenching. However, more detailed experiments are necessary to identify these decay channels and to confirm this interpretation. The spectroscopy mode of the PEEM and the STM will help to efficiently distinguish between single electron excitation properties and LSP properties. An advantage is also the potential to locally correlate time-resolved PEEM, SEM and also STM [24]. As of now, we are able to correlate photoemission signatures in the PEEM images to areas in the SEM image containing about 10 clusters. For optimized substrate conditions that allow us to apply the full resolution potential of the PEEM (maximum extractor voltage) we expect that such a correlation should even be possible with an accuracy of a single cluster. Furthermore, the use of a gas-aggregation cluster source for these experiments will enable a better control of the cluster properties including a homogeneous deposition of the clusters with respect to cluster size and independent of the substrate properties. By this means an efficient discrimination between cluster-substrate coupling effects and cluster size effects will become possible.

5 Summary

We have investigated local variations in the femtosecond dynamics with nanometer resolution associated with electronic excitations in silver clusters as governed by inhomogeneities of the supporting HOPG substrate. A highly local and defined control of these inhomogeneities could be achieved by a nanoscale preparation of the substrate using the focused ion beam technique. The complementary use of STM, SEM and time-resolved PEEM enabled us to identify the potential microscopic mechanisms responsible for the local differences in the ultrafast cluster dynamics.

We thank our co-workers at the Raith GmbH for their help with the FIB structuring of the HOPG samples using the ionLiNE instrument. This work was supported by the Deutsche Forschungsgemeinschaft through SPP 1153.

References

1. B. Lamprecht, A. Leitner, F.R. Aussenegg, Appl. Phys. B **68**, 419 (1999)
2. F. Stietz, J. Bosbach, T. Wenzel, T. Vartanyan, A. Goldmann, F. Träger, Phys. Rev. Lett. **84**, 5644 (2000)
3. M. Scharte, R. Porath, T. Ohms, J.R. Krenn H. Ditlbacher, F.R. Aussenegg, A. Liebsch, M. Aeschlimann, Appl. Phys. B **73**, 305 (2001)
4. H. Hövel, B. Grimm, M. Pollmann, B. Reihl, Phys. Rev. Lett. **81**, 4608 (1998)
5. M. Merschdorf, C. Kennerknecht, K. Willig, W. Pfeiffer, New J. Phys. **4**, 95.1 (2002)
6. M. Merschdorf, W. Pfeiffer, S. Voll, G. Gerber, Phys. Rev. B **68**, 155416 (2003)
7. M. Aeschlimann, Review in *Encyclopedia of Nanoscience and Nanotechnology*, volume 3, edited by H. Nalwa (American Scientific Publishers, 2004), pp. 29–40

8. H. Hövel, S. Fritz, A. Hilger, U. Kreibig, M. Vollmer, Phys. Rev. B **48**, 18178 (1993)
9. H. Hövel, I. Barke, H.-G. Boyen, P. Ziemann, M.G. Garnier, P. Oelhafen, Phys. Rev. B **70**, 045424 (2004)
10. J. Lange, D. Bayer, M. Rohmer, C. Wiemann, O. Gaier, M. Aeschlimann, M. Bauer, Proc. SPIE **6195**, 61950Z (2006)
11. O. Schmidt, M. Bauer, C. Wiemann, R. Porath, M. Scharte, O. Andreyev, G. Schönhense, M. Aeschlimann, Appl. Phys. B **74**, 223 (2002)
12. Ch. Ziethen, O. Schmidt, G.H. Fecher, C.M. Schneider, G. Schönhense, R. Frömter, M. Seider, K. Grzelakowski, M. Merkel, D. Funnemann, W. Swiech, H. Gundlach, J. Kirschner, J. Elec. Spec. Rel. Phenom. **88**, 983 (1998)
13. W. Swiech, G.H. Fecher, Ch. Ziethen, O. Schmidt, G. Schönhense, K. Grzelakowski, C.M. Schneider, R. Frömter, H.P. Oepen, J. Kirschner, J. Elec. Spec. Rel. Phenom. **84**, 171 (1997)
14. W. Pfeiffer, C. Kennerknecht, M. Merschdorf, Appl. Phys. A **78**, 1011 (2004)
15. J. C. Diels, *Ultrashort Laser Pulse Phenomena* (Academic Press, 1995)
16. T. Becker, H. Hövel, M. Tschudy, B. Reihl, Appl. Phys. A **66**, S27 (1998)
17. H. Hövel, Th. Becker, A. Bettac, B. Reihl, M. Tschudy, E.J. Williams, J. Appl. Phys. **81**, 154 (1997)
18. R.G. Forbes, Vacuum, **48**, 85 (1997)
19. V.E. Krohn, J. Appl. Phys. **45**, 1144 (1974)
20. F. Ghaleh, R. Köster, H. Hövel, L. Bruchhaus, S. Bauerdick, J. Thiel, R. Jede, J. Appl. Phys. **101**, 044301 (2007)
21. R.L. Seliger, J.W. Ward, V. Wang, R.L. Kubena, Appl. Phys. Lett. **34**, 310 (1979)
22. J. Gierak, D. Mailly, P. Hawkes, R. Jede, L. Bruchhaus, L. Bardotti, B. Prével, P. Mélinon, A. Perez, R. Hyndman, J.-P. Jamet, J. Ferré, A.Mougin, C. Chappert, V. Mathet, P. Warin, J. Chapman, Appl. Phys. A **80**, 187 (2005)
23. M. Munzinger, C. Wiemann, M. Rohmer, L. Guo, M. Aeschlimann, M. Bauer, New J. Phys. **7**, 68 (2005)
24. M. Rohmer, C. Wiemann, M. Munzinger, L. Guo, M. Aeschlimann, M. Bauer, Appl. Phys. A **82**, 87 (2006)
25. M. Aeschlimann, M. Bauer, S. Pawlik, Chem. Phys. **205**, 127 (1996)
26. U. Höfer, I.L. Shumay, Ch. Reuß, U. Thomann, W. Wallauer, Th. Fauster, Science **277**, 1480 (1997)
27. M. Bauer, S. Pawlik, M. Aeschlimann, Phys. Rev. B **55**, 10040 (1997)
28. L.D. Landau, E.M. Lifschitz, *Lehrbuch der Theoretischen Physik, Bd. II: Klassische Feldtheorie, 6. Auflage* (Akademie-Verlag Berlin, 1973)